PAPER

Check for updates

Electronic structure and lattice dynamics of Ba$_2$CuTeO$_6$ single crystals†‡

Yun Chen Chung,[a] Sunil K. Karna,[b] Fan-Cheng Chou [ID] [b] and Hsiang-Lin Liu [ID] *[a]

The electronic structure and lattice dynamics of Ba$_2$CuTeO$_6$ single crystals were investigated through spectroscopic ellipsometry and Raman scattering measurements. The room-temperature optical absorption spectrum of Ba$_2$CuTeO$_6$ presented a direct optical band gap at approximately 1.04 eV and exhibited four bands at approximately 1.45, 3.43, 4.65, and 5.79 eV. The optical absorption band at 1.45 eV was attributed to on-site Cu^{2+} d–d transition. The other bands were attributed to charge-transfer transitions between the O 2p and Cu 3d or Te 5p states. The room-temperature Raman scattering spectrum of Ba$_2$CuTeO$_6$ exhibited 16 phonon modes at approximately 85, 97, 104, 119, 160, 194, 380, 396, 404, 409, 492, 568, 574, 606, 679, and 751 cm^{-1}. When the temperature decreased to less than 287 K, which is the temperature at which structural phase transition occurs from the monoclinic phase to the triclinic phase, additional phonon modes appeared at approximately 124, 128, 152, and 601 cm^{-1}. On further cooling to lower than 75 and 15 K, which are the temperatures at which short- and long-range antiferromagnetic phase transitions occur, respectively, the phonon modes at approximately 97, 104, 124, 128, 152, 160, 194, 380, 396, 409, 568, 574, 606, and 679 cm^{-1} exhibited softening, which indicates a coupling between the magnetic and lattice degrees of freedom. The stretching vibration of CuO$_6$ octahedra located at 679 cm^{-1} had the largest spin–phonon coupling constant (1.67 mRy Å^{-2}).

I. Introduction

Double perovskite Ba$_2$CuTeO$_6$ has attracted considerable research interest because of its complex physical properties, such as structural phase transition,[1,2] low-dimensional magnetism with $S = 1/2$ Cu^{2+} ions accompanied by magnetic phase transitions,[3] and quantum criticality.[4] It consists of CuO$_6$ octahedra that are linked with corner-shared and face-shared TeO$_6$.[1,2,4–6] The room-temperature crystal structure of Ba$_2$CuTeO$_6$ is monoclinic. Ba$_2$CuTeO$_6$ undergoes a structural phase transition to the triclinic structure at approximately 287 K (ref. 4, 7 and 8) and exhibits magnetic phase transitions at approximately 75 and 15 K.[1] When the temperature decreases to 75 K, the $S = 1/2$ Cu^{2+} ions form complex-couple Cu–O–Te–O–Cu superexchange paths. Ba$_2$CuTeO$_6$ exhibits short-range antiferromagnetic (AF) correlations.[1] A long-range AF ordering is observed at 15–16 K. The two-leg ladders have strong interladder couplings, which render the Néel-ordered ground state stable.[7] The crystal and magnetic phase transitions of Ba$_2$CuTeO$_6$ are presented in Fig. 1.

[a]Department of Physics, National Taiwan Normal University, Taipei 11677, Taiwan. E-mail: hliu@ntnu.edu.tw

[b]Center for Condensed Matter Sciences, National Taiwan University, Taipei 10617, Taiwan

† Electronic supplementary information (ESI) available. See DOI: 10.1039/d0ra02314k

‡ PACS numbers: 71.27.+a, 71.35.Cc, 78.30.-j.

Although considerable research has been conducted on Ba$_2$CuTeO$_6$, its optical and phonon properties have remained relatively unexplored. Rao et al.[1] performed the first-principles calculations and predicted a direct band gap energy of 1.0 eV for Ba$_2$CuTeO$_6$. Glamazda et al.[8] examined the polarized Raman
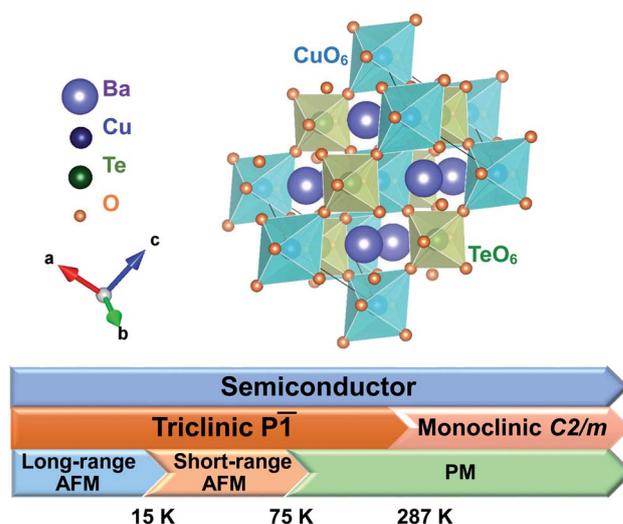

Fig. 1 Crystal structure of Ba$_2$CuTeO$_6$ at low temperatures. Schematic depicting the electric, structural, and magnetic properties of Ba$_2$CuTeO$_6$ (AFM: antiferromagnetic and PM: paramagnetic).

scattering spectra of Ba_2CuTeO_6 as a function of temperature. They found that the two-magnon Raman response of Ba_2CuTeO_6 exhibits linear temperature dependence in its peak energy, linewidth, and intensity over a wide range of temperatures. This scaling behavior suggests that Ba_2CuTeO_6 is close to a quantum-critical point from an ordered side. In this study, we used spectroscopic ellipsometry and Raman scattering measurements to investigate the electronic structure and lattice dynamics of Ba_2CuTeO_6. We observed a direct optical band gap near 1.04 eV at room temperature and four optical excitations at approximately 1.45, 3.43, 4.65, and 5.79 eV. Furthermore, we noted 16 Raman-active phonon modes. When the temperature was decreased, anomalous results were observed at temperatures lower than 75 K for the position and strength of the phonon modes at approximately 97, 104, 124, 128, 152, 160, 194, 380, 396, 409, 568, 574, 606, and 679 cm^{-1}, which can be attributed to spin–phonon coupling-induced phonon renormalization.

II. Experiment

Single-crystal Ba_2CuTeO_6 samples were grown through the flux method by using $BaCl_2$ as the flux. A mixture of the polycrystalline sample of Ba_2CuTeO_6 and the flux of $BaCl_2$ (molar ratio, 1 : 3) was melted in an alumina crucible at 1150 °C for 24 h. The furnace was slowly cooled to 850 °C at a rate of 3 °C h^{-1} and then cooled to room temperature at a rate of 80 °C h^{-1}. Dark green crystals (1–3 mm) were mechanically separated from the crucible and then washed with hot water.[1] The crystal structure and phase purity of the samples were examined through synchrotron X-ray powder diffraction.[1] Spectroscopic ellipsometry measurements were conducted at an incidence angle of 75° by using a Woollam M-2000U ellipsometer over a spectral range of 0.73–6.42 eV. The experimental data were measured reproducibly at three spots (100×100 μm^2) on the sample surface by using a specially designed focusing optics system coupled with an ellipsometer. Lorentz approximation was used to fit the raw ellipsometry data and calculate the dielectric function. Micro-Raman scattering experiments were conducted with a backscattering geometry by using a diode-pumped solid-state laser at an excitation wavelength of 532 nm. We focused linearly polarized light on the sample through a 50× optical microscope objective (numerical aperture: 0.75) with a spatial resolution of 3 μm. To avoid heating effects, the laser power used was less than 1 mW. The scattered light, which was not subject to polarization analysis, was collected and dispersed using a SENTERRA spectrometer equipped with a 1024-pixel-wide charge-coupled detector. The spectral resolution with this spectrometer is typically less than 0.5 cm^{-1}. The polarized Raman scattering spectra were obtained in backscattering geometry from four scattering configurations, namely $Z(Y, Y)Z$, $Z(Y, X)Z$, $Z(Y', Y')Z$, and $Z(Y', X')Z$. In this Porto notation, the first and last letter represent the directions of the incident and scattered light, whereas the letters in parentheses indicate the polarizations of the incident and scattered light, respectively. X, Y, and Z are parallel to the orthorhombic [100], [010], and [001] crystal directions, whereas

X' and Y' are along [110] and [$\bar{1}$10] crystal directions, respectively. The sample was placed in a continuous helium flow cryostat, which allowed measurements to be conducted in the temperature range of 10–300 K.

III. Results and discussion

Fig. 2(a) presents the real (ε_1) and imaginary (ε_2) parts of the dielectric function $\varepsilon(\omega)$ of Ba_2CuTeO_6, which was obtained through spectroscopic ellipsometry analysis at room temperature. The dispersive response of ε_1 had a positive value, which was similar to the typical behavior of a semiconductor. The peak of ε_2 at approximately 4.0 eV leveled off at higher energies, which revealed that electromagnetic radiation was absorbed by Ba_2CuTeO_6 near 4.0 eV. Fig. 2(b) illustrates the optical absorption coefficient spectrum of Ba_2CuTeO_6 measured at room temperature. We fitted this absorption spectrum by using standard Lorentzian functions.[9] With an increase in photon energy, absorption increased progressively and four absorption bands were observed at approximately 1.45, 3.43, 4.65, and 5.79 eV. According to the previous first-principles calculations, the first absorption peak (the inset of Fig. 2(b)) was attributed to the on-site Cu^{2+} d–d transition. The other peaks were attributed
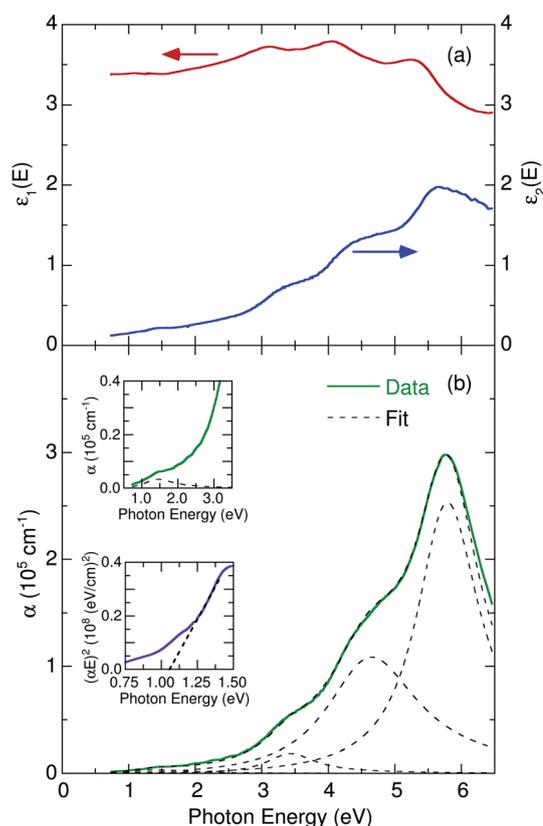

Fig. 2 (a) Dielectric function of Ba_2CuTeO_6 estimated at room temperature. (b) The optical absorption coefficient of Ba_2CuTeO_6 estimated at room temperature. The dashed lines show the optimal fit from the Lorentzian model. The inset illustrates the optical absorption coefficient in the low-energy region (0.5–3.5 eV) and the direct band gap analysis of Ba_2CuTeO_6.

to charge-transfer transitions from the oxygen 2p states to the copper 3d or tellurium 5p states.[1]

In a typical solid, the absorption coefficient includes contributions from the direct and indirect band gap transitions and is expressed as follows:[10,11]

$$\alpha(E) = \frac{A}{E}\left(E - E_{g,dir}\right)^{0.5} + \frac{B}{E}\left(E - E_{g,ind} \mp E_{ph}\right)^2, \qquad (1)$$

where $E_{g,dir}$ and $E_{g,ind}$ are the magnitudes of the direct and indirect band gaps, respectively, E_{ph} is the absorbed (emitted) phonon energy, and A and B are constants. The aforementioned model, which assumes a simple band shape, enables the extraction of the direct energy gap when $(\alpha E)^2$ is plotted as a function of the photon energy. The inset of Fig. 2(b) presents a direct band gap of 1.04 ± 0.01 eV at 300 K. Plotting $(\alpha E)^{0.5}$ as a function of photon energy led to an indirect band gap of about 0.24 eV (see ESI Fig. 1†). Our experimental result in the direct band gap analysis is in good agreement with the theoretical band structure calculations of Ba_2CuTeO_6, which yield a direct band gap energy of 1.0 eV.[1]

Fig. 3 depicts the room-temperature Raman scattering spectrum of Ba_2CuTeO_6. The spectrum comprises 16 first-order Raman phonon modes. We fitted these phonon peaks using standard Lorentzian functions.[9] We observed a total of 16 Raman-active phonon modes at room temperature at approximately 85, 97, 104, 119, 160, 194, 380, 396, 404, 409, 492, 568, 574, 606, 679, and 751 cm^{-1}. The inset illustrates the polarized Raman scattering spectra of Ba_2CuTeO_6 at room temperature in four configurations. The modes at 85, 97, 104, 119, 160, 194, 380, 396, 404, 409, 492, 568, 574, 606, 679, and 751 cm^{-1} exhibited a higher intensity in the parallel configuration (YY)
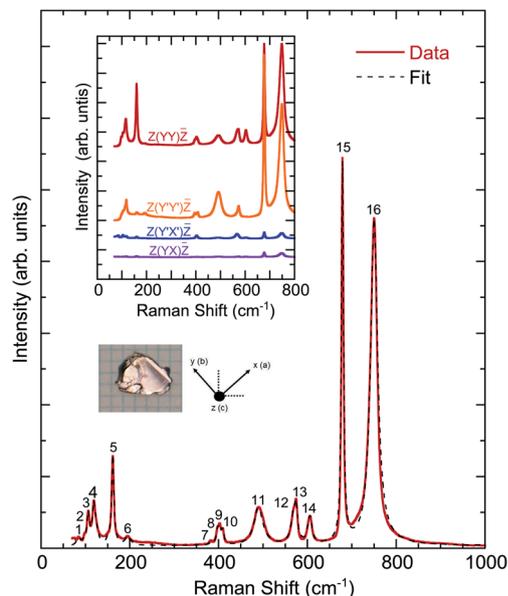
than in the cross configuration (YX). This satisfies the selection rule for $C2/m$ in which A_{1g} and B_{1g} modes should appear in the YY configuration and no peaks are expected for the YX configuration. On the other hand, the primed spectra Y′Y′ was different from its unprimed counterpart YY, which shows that the sample is a single crystal. The Y′Y′ spectrum showed the suppressed intensity of the modes approximately 160 and 606 cm^{-1}. We deduced that the 85, 97, 104, 119, 194, 380, 396, 404, 409, 492, 568, 574, 679, and 751 cm^{-1} phonon modes exhibited A_{1g} symmetry, whereas the 160 and 606 cm^{-1} phonon modes exhibited B_{1g} symmetry. According to factor group analysis, Ba_2CuTeO_6 has a monoclinic structure (space group $C2/m$)[8] that contains one formula unit per primitive cell at room temperature. The irreducible representation of the phonon modes at the center of the Brillouin zone is presented as follows: $\Gamma = 16A_g + 11B_g$.[8] In accordance with previous report,[8] the phonon peaks at approximately 85, 97, 104, 119, 160 and 194 cm^{-1} were assigned to the displacement of Ba atoms and the rotations of CuO_6 and the TeO_6 octahedra. The phonon peaks at approximately 380, 396, 404, 409, and 492 cm^{-1} were associated with the bending vibrations of CuO_6 and TeO_6 octahedra. The phonon peaks at approximately 568, 574, 606, 679, and 751 cm^{-1} were attributed to the stretching vibration of TeO_6 and CuO_6 octahedra.

The temperature-dependent Raman scattering spectra of Ba_2CuTeO_6 are depicted in Fig. 4. The inset illustrates the Raman scattering spectra between 75 and 150 cm^{-1}. At low temperatures, the irreducible representation of the phonon
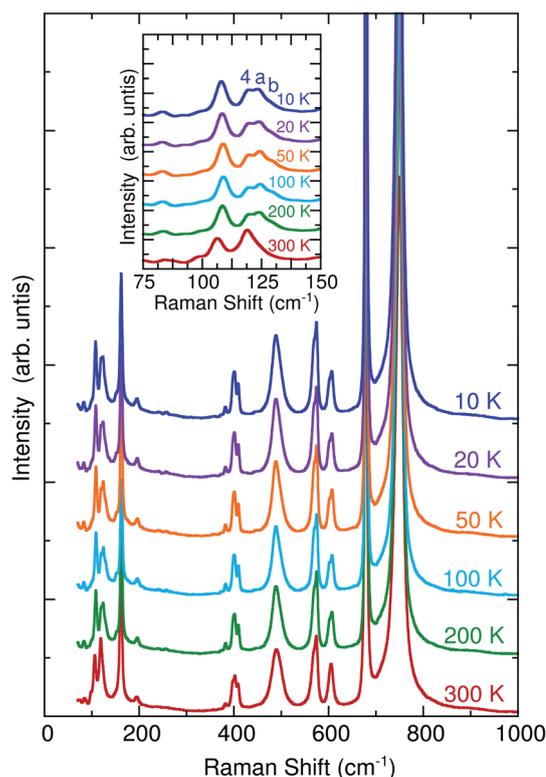

Fig. 3 Unpolarized Raman scattering spectrum of Ba_2CuTeO_6 measured at room temperature. The dashed line shows the fitting results of the spectrum obtained using the Lorentzian model. The inset illustrates the polarized Raman scattering spectra and the optical image of Ba_2CuTeO_6 single crystal. The notations used for the crystallographic directions are also given.

Fig. 4 Temperature dependence of Raman scattering spectra of Ba_2CuTeO_6. The inset indicates the Raman scattering spectra between 75 and 150 cm^{-1}.

modes at the center of the Brillouin zone is presented as $\Gamma = 27A_g$. In our investigation, we observed 20 phonon modes. New peaks appeared at approximately 124, 128, 152, and 601 cm^{-1} at low temperatures. Fig. 5 illustrates the new peaks that appeared between 120 and 130 cm^{-1} at low temperatures. The new peaks indicate that a weak crystal phase change occurred from the monoclinic state to the triclinic state.[2,8] With a decrease in temperature, these new phonon modes exhibited softening at temperatures lower than 75 K. Fig. 6 displays the temperature-dependent parameters (frequency, linewidth, and normalized intensity) of the phonon modes at 606 and 679 cm^{-1}. The temperature-dependent parameters of other phonon modes are provided in ESI Fig. 2.† The stretching vibrations of TeO$_6$ and CuO$_6$ octahedra near 606 and 679 cm^{-1} exhibited a blueshift when the temperature decreased to 200 K. When the temperature decreased to 75 K, which is the short-range AF phase transition temperature, the redshift and normalized intensities of the phonon modes increased. Our results differed from those of previous measurements.[8] Glamazda *et al.* did not observe the phonon anomalies at temperatures lower than the magnetic phase transition temperatures. One possibility that could account for this difference is due to the different growth processes,[1,8] resulting in different quality of single crystals.

The temperature dependence of the phonon frequency can be expressed as follows:[12]

$$\omega(T) = \omega_0 + A\left(1 + \frac{2}{\exp(\hbar\omega_0/2k_B T) - 1}\right), \quad (2)$$
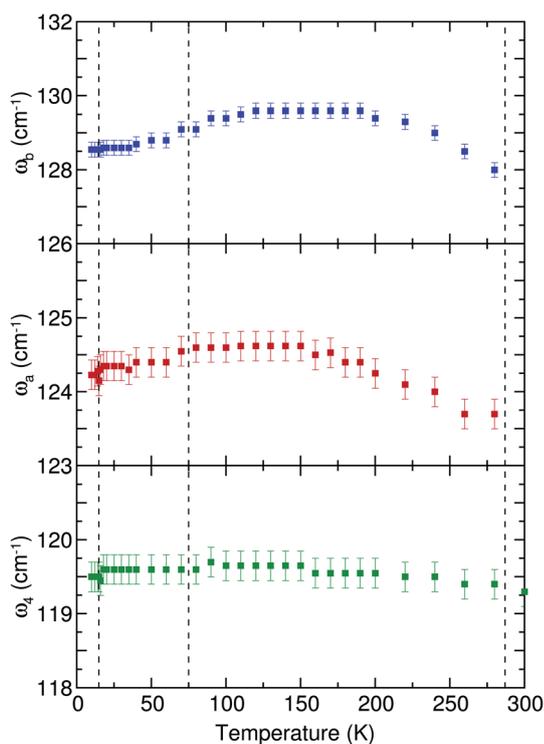

Fig. 5 Temperature dependence of phonon frequency near 119, 124, and 128 cm^{-1}.
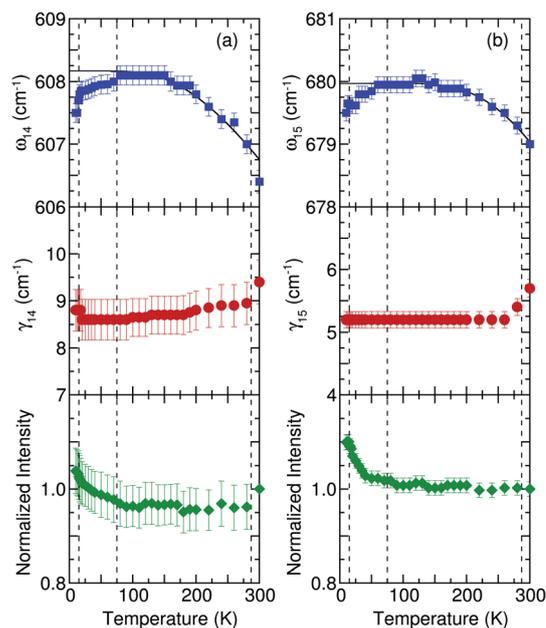

Fig. 6 Temperature dependence of frequency, linewidth, and normalized intensity of (a) 606 and (b) 679 cm^{-1} phonon modes. The vertical dashed lines indicate the magnetic phase transition temperatures at 15 K, 75 K and structure phase transition at 287 K. The thin solid line denotes the result of the fitting obtained using the anharmonic model.

where ω_0 is the intrinsic frequency of the optical phonon mode, parameter A is the anharmonic coefficient, and $\frac{1}{\exp(\hbar\omega_0/2k_B T) - 1}$ corresponds to the thermal population factor of acoustic modes. For the analysis of anharmonic contributions to the 606 cm^{-1} phonon modes, the values of ω_0 (approximately 615 cm^{-1}) and parameter A (approximately -6.8 cm^{-1}) were determined. For the 679 cm^{-1} phonon mode, the values of ω_0 (approximately 690 cm^{-1}) and parameter A (approximately -10 cm^{-1}) were determined. The thin solid lines in Fig. 6(a) and (b) represent the theoretical predictions based on eqn (2). The frequency of the stretching vibrations of the TeO$_6$ and CuO$_6$ octahedra deviated from the theoretical predictions at temperatures lower than 75 K. This phenomenon occurred because of a spin–phonon coupling in the AF state of Ba$_2$CuTeO$_6$.

In a magnetic material, the temperature-dependent frequency change of the phonon mode can be expressed as follows:[13]

$$\omega(T) = \omega_0 + \Delta\omega_{\text{latt}}(T) + \Delta\omega_{\text{anh}}(T) + \Delta\omega_{\text{e-ph}}(T) + \Delta\omega_{\text{s-ph}}(T), \quad (3)$$

where ω_0 is the harmonic frequency of the phonon; $\Delta\omega_{\text{latt}}(T)$ is the contribution of lattice expansion and contraction to the phonon frequency; $\Delta\omega_{\text{anh}}(T)$ is the intrinsic anharmonic contribution; $\Delta\omega_{\text{e-ph}}(T)$ is the contribution due to the renormalization effect of the phonon frequency that results from electron–phonon coupling, which could be negligible in Ba$_2$CuTeO$_6$; and $\Delta\omega_{\text{s-ph}}(T)$ is the spin–phonon coupling contribution caused by lattice

Table 1 Spin–phonon coupling constants for 14 phonon modes

Mode frequency (cm^{-1})	Spin–phonon coupling constant ($mRy\ Å^{-2}$)
97	0.39
104	0.76
124	0.40
128	0.38
152	0.37
160	0.56
194	0.51
380	0.56
396	1.27
409	0.60
568	0.56
574	0.88
606	1.49
679	1.67

vibrations due to the modulation of the exchange integral. The magnetic coupling among Cu spins is expected to be established through the Cu–O–Te–O–Cu superexchange path. Spin correlations develop when the temperature decreases to 75 K. We calculated $\Delta\omega_{s-ph}$ from the frequency-shift data by using the following expression:[14]

$$\Delta\omega_{s-ph} = -\frac{1}{\omega_0}\left(\lambda_{eff}\right)\left[\frac{M_{sub}(T)}{4\mu_B}\right]^2, \qquad (4)$$

where λ_{eff} is the spin–phonon coupling constant and $M_{sub}(T)$ is the sublattice magnetic susceptibility. We used the magnetic susceptibility[1] to estimate the spin–phonon coupling constant for all redshifted phonon modes. The spin–phonon coupling constants are listed in Table 1. These values were one order of magnitude lower than those obtained for perovskite oxides,[15–20] thus reflecting a weak spin-phonon coupling in Ba_2CuTeO_6.

IV. Summary

We used spectroscopic ellipsometry and Raman scattering spectroscopy to investigate the electronic and phononic excitations of Ba_2CuTeO_6. The direct optical band gap was found to be 1.04 eV. The optical absorption band at approximately 1.45 eV was attributed to on-site Cu^{2+} d–d transition. The other bands at approximately 3.43, 4.65, and 5.79 eV were attributed to charge-transfer transitions between the O 2p and Cu 3d or Te 5p states. Anomalies in the phonon frequency and intensity were detected at approximately 75 K, which indicated a spin–phonon coupling in Ba_2CuTeO_6. The stretching vibration of CuO_6 octahedra located at 679 cm^{-1} exhibited the largest spin–phonon coupling constant (1.67 $mRy\ Å^{-2}$).

Author contributions

H. L. L. conceived the idea and designed the experiments. Y. C. C. performed the experiments. S. K. K. and F. C. C. prepared the samples. Y. C. C. and H. L. L. wrote the paper. All the authors discussed the results and commented on the manuscript.

Data availability statement

The data that support the findings of this study are available from the corresponding author upon reasonable request.

Conflicts of interest

The authors declare no competing interests.

References

1 G. N. Rao, R. Sankar, A. Singh, I. P. Muthuselvam, W. T. Chen, V. N. Singh, G.-Y. Guo and F. C. Chou, Tellurium-bridged two-leg spin ladder in Ba_2CuTeO_6, *Phys. Rev. B*, 2016, **93**, 104401.

2 V. P. Köhl and D. Reinen, Strukturelle und spektroskopische Untersuchungen am Ba_2CuTeO_6, *Z. Anorg. Allg. Chem.*, 1974, **409**, 257.

3 V. P. Köhl, U. Müller and D. Reinen, Ba_2NiTeO_6 – eine neue Verbindung in der Reihe der hexagonalen Perovskite, *Z. Anorg. Allg. Chem.*, 1972, **392**, 124.

4 A. S. Gibbs, A. Yamamoto, A. N. Yaresko, K. S. Knight, H. Yasuoka, M. Majumder, M. Baenitz, P. J. Saines, J. R. Hester, D. Hashizume, A. Kondo, K. Kindo and H. Takagi, S = 1/2 quantum critical spin ladders produced by orbital ordering in Ba_2CuTeO_6, *Phys. Rev. B*, 2017, **95**, 104428.

5 R. L. Moreira, R. P. S. M. Lobo, S. L. L. M. Ramos, M. T. Sebastian, F. M. Matinaga, A. Righi and A. Dias, Raman and infrared spectroscopic investigations of a ferroelastic phase transition in Ba_2ZnTeO_6 double perovskite, *Phys. Rev. Mater.*, 2018, **2**, 054406.

6 D. Iwanaga, Y. Inaguma and M. Itoh, Crystal structure and magnetic properties of B′-site ordered perovskite-type oxides $A_2CuB'O_6$ (A = Ba, Sr; B′ = W, Te), *J. Solid State Chem.*, 1999, **147**, 291.

7 D. Macdougal, A. S. Gibbs, T. Ying, S. Wessel, H. C. Walker, D. Voneshen, F. Mila, H. Takagi and R. Coldea, Spin dynamics of coupled spin ladders near quantum criticality in Ba_2CuTeO_6, *Phys. Rev. B*, 2018, **98**, 174410.

8 A. Glamazda, Y. S. Choi, S.-H. Do, S. Lee, P. Lemmens, A. N. Ponomaryov, S. A. Zvyagin, J. Wosnitza, D. P. Sari, I. Watanabe and K.-Y. Choi, Quantum criticality in the coupled two-leg spin ladder Ba_2CuTeO_6, *Phys. Rev. B*, 2017, **95**, 184430.

9 F. Wooten, Optical Properties of Solids, *Ann. Phys.*, 1935, **24**, 636.

10 J. I. Pankove, *Optical Processes in Semiconductors*, Dover, New York, 1971.

11 H. L. Liu, C. R. Huang, G. F. Luo and W. N. Mei, Optical properties of antiferroelectric $Cs_2Nb_4O_{11}$: Absorption spectra and first-principles calculations, *J. Appl. Phys.*, 2011, **110**, 103515.

12 J. Menéndez and M. Cardona, Temperature dependence of the first-order Raman scattering by phonons in Si, Ge, and $\alpha-Sn$: Anharmonic effects, *Phys. Rev. B: Condens. Matter Mater. Phys.*, 1984, **29**, 2051.

13 J. Xu, J. H. Park and H. M. Jang, Orbital-spin-phonon coupling in Jahn-Teller-distorted $LaMnO_3$: Softening of the 490 and 610 cm^{-1} Raman-active modes, *Phys. Rev. B: Condens. Matter Mater. Phys.*, 2007, **75**, 012409.

14 W. Baltensperger and J. S. Helman, Influence of magnetic order in insulators on the optical phonon frequency, *Helv. Phys. Acta*, 1968, **41**, 668.

15 J. Vermette, S. Jandl and M. M. Gospodinov, Raman study of spin–phonon coupling in $ErMnO_3$, *J. Phys.: Condens. Matter*, 2008, **20**, 425219.

16 E. Granado, A. García, J. A. Sanjurjo, C. Rettori, I. Torriani, F. Prado, R. D. Sánchez, A. Caneiro and S. B. Oseroff, Magnetic ordering effects in the Raman spectra of $La_{1-x}Mn_{1-x}O_3$, *Phys. Rev. B: Condens. Matter Mater. Phys.*, 1999, **60**, 11879.

17 J. Laverdiere, S. Jandl, A. A. Mukhin, V. Y. Ivanov, V. G. Ivanov and M. N. Illiev, Spin-phonon coupling in orthorhombic $RMnO_3$ (R = Pr, Nd, Sm, Eu, Gd, Tb, Dy, Ho, Y): A Raman study, *Phys. Rev. B: Condens. Matter Mater. Phys.*, 2006, **73**, 214301.

18 H. S. Hsu, F. C. Chou, K. Koyama, K. Watanabe and H. L. Liu, Spin-phonon coupling in antiferromagnetic $Bi_2Sr_2CoO_{6+\delta}$: An infrared reflectance study, *Phys. Rev. B: Condens. Matter Mater. Phys.*, 2009, **79**, 155109.

19 S. Issing, A. Pimenov, V. Yu. Ivanov, A. A. Mukhin and J. Geurts, Composition-dependent spin-phonon coupling in mixed crystals of the multiferriuc manganite $Eu_{1-x}Y_xMnO_3$ ($0 \leq x \leq 0.5$) studied by Raman spectroscopy, *Phys. Rev. B: Condens. Matter Mater. Phys.*, 2010, **81**, 024304.

20 H. W. Chen, Y.-W. Chen, J.-L. Kuo, Y. C. Lai, F. C. Chou, C. H. Du and H. L. Liu, Spin-charge-lattice coupling in $YBaCuFeO_5$: Optical properties and first-principles calculations, *Sci. Rep.*, 2019, **9**, 3223.